ROYAL SOCIETY
OF CHEMISTRY

PAPER

Check for updates

Thermal decomposition of nano Al-based energetic composites with fluorinated energetic polyurethane binders: experimental and theoretical understandings for enhanced combustion and energetic performance†

Gang Tang,[a] He Wang,[b] Chunyan Chen,[c] Yabei Xu,[b] Dongping Chen,*[b] Dongli Wang,[a] Yunjun Luo 🅾 *[ad] and Xiaoyu Li 🅾 *[ade]

Energetic composites composed of polymeric binders and metallic fuels are widely used in industrial and military fields, and their performance is largely dependent on the combustion process. Fluorinated energetic polymeric binders can facilitate the combustion of metallic fuels such as aluminum particles and enhance the energetic level of the energetic composites. In this report, fluorinated energetic polyurethanes (FPUs) were applied as binders for energetic composites with aluminum nanoparticles (AlNPs). The fluorinated components in the energetic binder could be a uniform dispersion inside the composites, endowing the composites with decent mechanical properties and high combustion rate. Most significantly, compared with the composites without fluorine, FPU/AlNP energetic composites not only showed a remarkably improved combustion efficiency, but also, surprisingly, a dramatic enhancement in the heat of explosion by 91.2%, despite the low content of fluorine. By analyzing the combustion products together with kinetic simulations derived from chemical reaction neural network (CRNN) modelling, a detailed mechanistic understanding of the combustion process was provided, suggesting the importance of synergistic effects brought by the fluorinated and energetic components.

Introduction

Energetic materials composed of polymeric binders and metallic fuels are widely applied in industrial and military fields, such as propellants, explosives, pyrotechnics *et al.*[1–5] Metallic fuels, such as aluminum, are widely used in energetic composites to enhance the comprehensive performance, such as energy level,[6] combustion temperature,[7] density,[8,9] and so on. Nevertheless, aluminum particles in energetic composites often suffer from incomplete combustion and easy agglomeration, leading to reduced energy release and combustion efficiency. To overcome these problems, one of the efficient strategies is to introduce fluoropolymers into energetic composites.[10] In 1956,

the first example of the application of fluoropolymer (poly-chlorotrifluoroethylene) and magnesium fuels in pyrotechnics was reported.[11] Since then, numerous metal/fluoropolymer composites have been developed and widely applied in energetic materials.[12,13] During combustion, aluminum is oxidized, and energy is released upon the formation of fluorine–aluminum bonds.[14] Moreover, fluoropolymer oxidizers are increasingly prevalent in the development of energetic materials due to their higher densities.

Despite these advantages, direct blending of fluorinated polymers could drastically impair mechanical properties due to their low compatibility with other components and reduces the overall energy level of energetic materials,[15] which is hindered for their practical applications. Moreover, although the thermal decomposition of energetic polymer/metal and fluorinated polymer/metal composites have both been explored previously, the combination of these two components in one energetic binder has not been comprehensively investigated due to the complicated combustion mechanism. Therefore, a comprehensive understanding of the energetic composites using the fluorinated energetic polymer as binder, including their energy level, mechanical properties and combustion mechanism is absent. In addition, in order to deeply understand the thermal decomposition process of energetic materials, the commonly

[a] *School of Materials Science and Engineering, Beijing Institute of Technology, Beijing, 100081, China. E-mail: yjluo@bit.edu.cn; xiaoyuli@bit.edu.cn*

[b] *State Key Lab of Explosion Science and Technology, Beijing Institute of Technology, Beijing, 100081, China. E-mail: dc516@bit.edu.cn*

[c] *Xi'an Modern Chemistry Research Institute, Xi'an, 710065, China*

[d] *Key Laboratory of High Energy Density Materials, Ministry of Education, Beijing Institute of Technology, Beijing, 100081, China*

[e] *Experimental Center of Advanced Materials, Beijing Institute of Technology, Beijing 100081, China*

† Electronic supplementary information (ESI) available. See https://doi.org/10.1039/d2ra03781e

used kinetic models are Kissinger,[16] Friedman,[17] Ozawa,[18] Starink,[19] and chemical reaction neural network (CRNN).[20–23] The CRNN uses the network model to solve the reaction kinetics equation, and can propose the multi-step overall reaction mechanism, which can deeply understand the thermal decomposition kinetics of complex systems.

Herein, a series of fluorine-containing glycidyl azide polymer-based polyurethanes (FPUs) with different fluorine contents were synthesized. The application of the FPUs as binders for energetic composites with aluminum nanoparticles (AlNPs) endowed the composites with decent and tunable mechanical properties, which is thus highly desired for practical applications. Meanwhile, the incorporation of both the energetic component and fluorinated component into one polyurethane ensured the uniform dispersion of these two components inside the composites, not only facilitating the homogeneity of the combustion reaction but also the energy propagation in the AlNPs. The results from our combustion experiments unambiguously showed that the FPUs could dramatically enhance the energy release by 91.2%, and significantly improve the combustion efficiency of the AlNPs in energetic composites. Lastly, kinetic simulations of thermal decomposition were carried out *via* chemical reaction neural network (CRNN) model, together with the analysis of combustion products, to illustrate the combustion process in details. Our results strongly suggest that the both fluorinated and energetic components in these polyurethanes work synergistically during the combustion, which is crucial for their extraordinary performance improvement.

Experimental section

Materials and techniques

The glycidyl azide polymer (GAP, –OH equivalent, 28.14 mg KOH g^{-1}) was obtained from Liming Research Institute of Chemical Industry (Henan, China), and dried under vacuum at 90 °C for 4 h before use. The dicyclohexylmethylmethane-4, 4′-diisocyanate (HMDI, 98%, Shanghai Aladdin Bio-Chem Technology Co., Ltd) was used as received. The catalyst was prepared by dissolving dibutyltin dilaurate (DBTDL, 95%, Alfa Chemical Reagent Co., Ltd) in dibutyl phthalate at a concentration of 4.8 mg mL^{-1}. The fluorinated chain extender 2, 2, 3, 3-tetrafluoro-1, 4-butanediol (F4, 95%) was obtained from TCI chemicals Co., Ltd, and was used after vacuum drying at 40 °C for 4 h. The non-fluorinated chain extender 1, 4-butanediol (BDO, 99%) was obtained from Sigma-Aldrich and was used after vacuum drying at 60 °C for 48 h. Tetrahydrofuran (THF, 99%, Beijing Tongguang Fine Chemical Co., Ltd) was used after distillation over CaH$_2$. Aluminum nanoparticles (AlNPs) with an average diameter of 100 nm and an oxide shell (~2–4 nm) were purchased from Maoguo Nano Technology Co., Ltd (Shanghai, China).

Thermo gravimetric analysis (TG) was performed on a TG analyzer (TG/DSC1SF/417–2, Mettler Toledo). The energetic composites (0.5–1 mg) in platinum crucibles were heated from 30 °C to 900 °C at a scan rate of 10 K min^{-1} under argon flow (40 mL min^{-1}).

High-pressure differential scanning calorimetric analysis (HP-DSC) was carried out on a Mettler HP-DSC 2+. The composites (0.5–1 mg) in platinum crucibles were heated from 30 °C to 700 °C at a scan rate of 10, 20, 30 and 40 K min^{-1} under argon flow (50 mL min^{-1}). The test pressure used were 2, 4, 6 and 8 MPa.

The stress–strain test of the FPUs and energetic composites was carried out on a tensile testing machine (Instron-6022, Shimadzu Co. Ltd) at a constant strain rate of 100 mm min^{-1} at 25 °C. The dimensions of the samples were 20 mm (neck area length) × 4 mm (width) × 2 mm (thickness).

Scanning electron microscopic images (SEM) were obtained from Hitachi SU8010 Field Emission SEM equipped with energy dispersive X-ray spectroscopy (EDS). Before the test, all samples were fractured in liquid nitrogen and coated with a layer of Pt (thickness ~10 nm).

The heat of explosion was detected by Parr 6200 bomb calorimetry (Illinois, USA). The test was carried out under argon atmosphere with a pressure of 2.36 MPa, and 1 g of sample was used for each test. Each sample was measured for three times and the average values were reported.

Powder X-ray diffraction (XRD) patterns were recorded using a Bruker D8 advance particle X-ray diffractometer featuring a filtered Cu Kα radiation ($\lambda = 1.5418$ Å). All tested samples were scanned at a scan rate of 0.5 s/step between 2θ angles from 20° to 100°.

Preparation of the energetic polyurethane

The fluorine-free energetic polyurethane (BPU-98-30) was synthesized according to literature.[24] The molar ratio between –NCO and –OH groups (R value) of BPU-98-30 is 0.98 and the hard segment contents is 30% (wt%). The fluorinated energetic polyurethane (FPUs) with different fluorine contents were synthesized according to literature,[25] except F4 was used for the chain extenders during the polymerization. The R value of the FPUs is 0.98, the hard segment contents are 30%, 35%, 40%, 45% and 50% (wt%), respectively.[26] The FPUs were named as FPU-X-Y, with "X" representing their R value × 100 and "Y" for their hard segment content (wt%) × 100. For example, FPU-98-30 stands for the FPU with an R value of 0.98, and a hard segment content of 30%.

Preparation of energetic composites

Desired amount of AlNPs was dispersed in THF *via* ultrasonication for 2 h at 28 °C to form a suspension with a weight concentration of 150 mg mL^{-1}. Considering the low fluorine content in FPUs, the content of aluminum in practical application, and the effect between fluorine with aluminum can be better reflected, all the FPUs/AlNPs energetic composites are aluminum excess. Therefore, the mass ratio between FPUs/AlNPs or BPU/AlNPs was fixed to 4.0. All FPUs or BPU were fully dissolved in THF at 60 °C for 6 h. The AlNPs suspension was mixed with the FPUs or BPU solution, and the mixture was further stirred at 60 °C for 2 h. The mixture was poured into a polytetrafluoroethylene beaker to remove the THF in a vacuum oven at 60 °C for 24 h. Then the energetic composites were

calendered *via* an oil heated double roll calender at 60 °C for 30 min to ensure the uniform distribution of AlNPs in the final FPUs/AlNPs and BPU/AlNPs energetic composites.

Kinetic simulations

The chemical reaction neural network (CRNN) modelling method was adopted to elucidate the reaction pathways and kinetic parameters by fitting the thermogravimetric experimental data. A detailed description of the methods is included in the ESI (Fig. S1–S4, Tables S1 and 2†).

Results and discussion

Preparation and mechanical properties of the energetic composites

The BPU and FPUs with different hard segment content were further used as binders and mixed with AlNPs to produce energetic composites. Aluminum particles with diameters of ~100 nm were chosen here, considering their higher reactivity toward the fluorinated component.[27,28] The SEM images of AlNPs are shown in Fig. S5.† In Fig. 1, the composites were prepared by first mixing the AlNPs suspension into a THF solution of FPUs or BPU, followed by evaporation of the solvent. AlNPs sediment due to their higher density. Therefore, to ensure the uniform distribution of AlNPs in the composites, the mixture was calendered *via* a double roll calender for 30 min to obtain the energetic nanocomposites. The utilization of double roll calender ensured the production of well-defined composites (Fig. S6†), and a uniform distribution of AlNPs and fluorinated components, which was confirmed by observation of the fractured surface of the composite specimen (Fig. S7 and S8†).
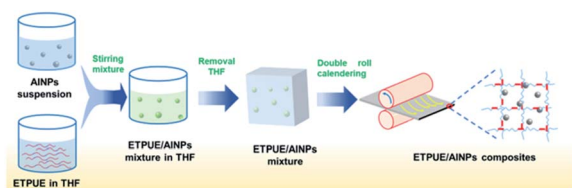

Fig. 1 Schematic illustration for the preparation process of FPUs/AlNPs and BPU/AlNPs composites.
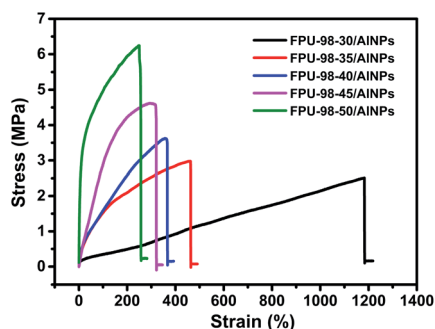

Fig. 2 Stress–strain curves of FPU-98-30/AlNPs to FPU-98-50/AlNPs.

Table 1 Mechanical test results of FPU-98-30/AlNPs to FPU-98-50/AlNPs

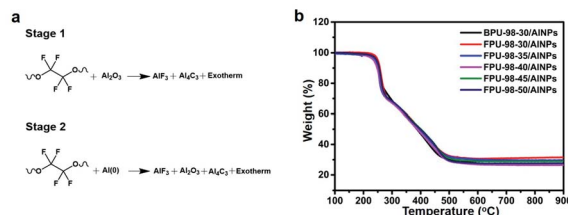| Samples	σ_m (MPa)	ε_b (%)
FPU-98-30/AlNPs	2.51 ± 0.35	1182.82 ± 56.24
FPU-98-35/AlNPs	2.98 ± 0.28	461.47 ± 27.66
FPU-98-40/AlNPs	3.53 ± 0.42	356.26 ± 45.34
FPU-98-45/AlNPs	4.58 ± 0.31	295.32 ± 56.42
FPU-98-50/AlNPs	6.15 ± 0.22	249.49 ± 39.18

Fig. 3 (a) Proposed thermal decomposition reactions of FPUs/AlNPs composites. (b) TG curves of the energetic composites, obtained at a scanning rate of 20 K min^{-1}.

The mechanical properties of these FPUs/AlNPs energetic composites were evaluated. It could be concluded from Fig. 2 and Table 1 that σ_m increased and ε_b decreased with increasing hard segment content, respectively. This trend observed for the composites agrees with that of FPUs. With the addition of AlNPs, all the resultant composites showed comparable values for σ_m and reduced values for ε_b. Nevertheless, all these energetic composites showed decent mechanical properties, which could be controlled by using different FPUs and might be useful for different practical applications.

Thermal decomposition of energetic composites

The FPUs could react with AlNPs, following the reaction schemes in Fig. 3a. The fluorocarbon units could react with both the aluminum and aluminum oxide layer on the surface. The thermal decomposition behaviors of these energetic composites were first characterized with a TG analyzer (TG-DSC) under argon. The TG curves from FPUs/AlNPs and BPU/AlNPs composites are shown in Fig. 3b. The TG results indicated that all the energetic composites started to thermally decompose at ~210 °C, corresponding to the decomposition of binders.

The TG-DSC curves from FPUs/AlNPs and BPU/AlNPs composites are shown in Fig. 4. The TG-DSC curves of BPU-98-30/AlNPs composites showed only one exothermic peak from the decomposition of the azide group. Meanwhile, those of the FPUs/AlNPs composites showed another obvious exothermic peak at approximately 500–800 °C, which could be attributed to the reaction between fluorine-containing components and residual carbon released from the decomposition of the FPUs, and alumina or aluminum.[29–32]

The results from TG-DSC can only provide qualitative analysis of the thermal decomposition process. To further study in
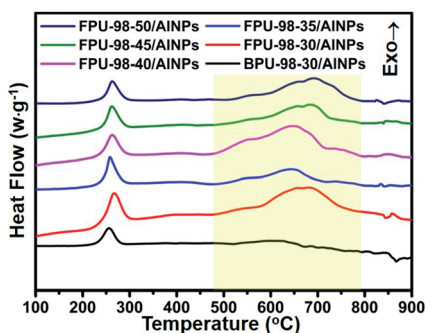
Fig. 4 TG-DSC curves of the energetic composites, obtained at a scanning rate of 20 K min^{-1}.
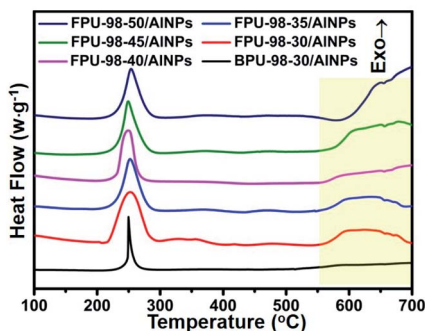

Fig. 5 HP-DSC curves of the composites obtained at a scanning rate of 20 K min^{-1} and pressure of 2 MPa.

a quantitative way, HP-DSC was applied to investigate the decomposition process of FPUs/AlNPs and BPU/AlNPs composites by varying the heating rate and pressure. Due to the limitation of the instrument, the maximum test temperature of the HP-DSC is 700 °C, and only the heat release below 700 °C could be recorded from the decomposition process of these energetic composites. In Fig. 5, the HP-DSC results also suggested that the decomposed product from FPUs could react with AlNPs to release a large amount of heat. In contrast, no obvious exothermic peak was observable for the BPU-98-30/AlNPs composites without fluorine.

Since both the heating rate and system pressure could significantly influence the combustion of the composite and thus the amount of gas released per unit time, the thermal

decomposition of FPU-98-50/AlNPs composites was studied with HP-DSC at different heating rates (Fig. 6a) and pressures (Fig. 6b). Fig. 6a shows that the amount of heat released by the reaction significantly increased when the heating rate increased from 10 to 40 K min^{-1}. Moreover, the setpoint of heat release shifted toward lower temperatures when the system pressure was increased from 2 to 8 MPa (Fig. 6b). The HP-DSC results indicated that a high heating rate and pressure are both beneficial to the combustion of AlNPs. Another thing noteworthy is that the so-called pre-ignition reaction (PIR) at 360 °C to 460 °C between fluorine and aluminum was not observed in any cases during thermal decomposition. This might be correlated with the low content of fluorine in the composite and also the short fluorocarbon chains of F4.[33]

Combustion of the energetic composites

The heat of explosion (ΔH_e) is the most important thermodynamic parameter for evaluating the performance of explosives and propellants.[34] Because GAP is an energetic polymer, all the energetic composites were ignited under argon by electrically heated nickel wires, and their ΔH_e values were evaluated via a bomb calorimeter. The results are shown in Table 2.

For the FPUs/AlNPs composites, ΔH_e only decreased slightly with an increasing hard segment content in the FPUs (Table 2). Surprisingly, the ΔH_e was increased dramatically from 1685 kJ kg^{-1} for the BPU-98-30/AlNPs composites to 3222 kJ kg^{-1} for the FPU-98-30/AlNPs composites. Considering the low weight content of fluorine in the composite (3.7%, Table 2), this enormous increase in ΔH_e (91.2% increase) was unexpected. Meanwhile, the similar chemical structure of fluorocarbon segments between F4 and PTFE, a similar enthalpy of the reaction between Al and FPUs to form AlF$_3$ in stoichiometric proportion could be assumed (-8.85 kJ g^{-1}).[35] Therefore, the additional energy released from the formation of AlF$_3$ was calculated to be 482, 593, 683, 784 and 885 kJ kg^{-1} for the composites from FPU-98-30, FPU-98-35, FPU-98-40, FPU-98-45, and FPU-98-50, respectively. These values are significantly smaller than the increase in ΔH_e from the combustion of bare FPUs to their corresponding composites. This finding suggests that the combustion of AlNPs might not only simply involve the exergonic reaction with the fluorinated component to form AlF$_3$, but also be promoted by other factors.

All the FPUs/AlNPs composites shared similarly high values of ΔH_e. Although the GAP energetic content in the FPUs decreased with increasing hard segment content, the fluorine
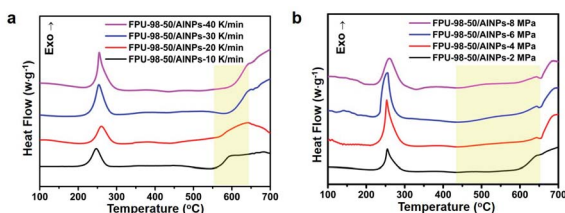

Fig. 6 HP-DSC curves of the FPU-98-50/AlNPs composites obtained (a) under a pressure of 2 MPa and at different scanning rates, and (b) at a scanning rate of 40 K min^{-1} and under different pressures.

Table 2 Heat of explosion for the FPUs/AlNPs and BPU/AlNPs composites

Samples	F (wt%)	Al (wt%)	ΔH_e (kJ kg^{-1})
BPU-98-30/AlNPs	0	20.00	1685 ± 14
FPU-98-30/AlNPs	3.70	20.00	3222 ± 11
FPU-98-35/AlNPs	4.55	20.00	2973 ± 50
FPU-98-40/AlNPs	5.24	20.00	2926 ± 19
FPU-98-45/AlNPs	6.02	20.00	3032 ± 48
FPU-98-50/AlNPs	6.79	20.00	3037 ± 83

content in the FPUs increased, and the fluorine-containing component resulted from decomposition of FPU could react with the AlNPs and release a large amount of heat, and promote other reactions. Therefore, the ΔH_e of the FPUs/AlNPs composites only decreased slightly with increasing hard segment content.

To provide a deep understanding of the complex combustion processes, the combustion products of these composites were retrieved from the bomb calorimeter and characterized with X-ray diffraction (XRD) (Fig. 7). The signal peaks of Al_2O_3, Al_4C_3, and $Al_2O_3 \cdot Al_4C_3$ were observed in the combustion products of all FPUs/AlNPs and BPU/AlNPs composites. However, the signal peaks of AlF_3 were only observed in the FPUs/AlNPs composites, and the signal peak intensity of AlF_3 gradually increased with increasing fluorine content in the FPUs, as expected. Moreover, the signals from bare Al_2O_3 were substantially reduced in the products from FPUs/AlNPs composites compared to those from BPU/AlNPs composite. Most importantly, the signal peak intensity of the remaining Al from the combustion product of FPUs/AlNPs composites, if not negligible, was tremendously lower than that from BPU-98-30/AlNPs composites. This finding is exciting and plausive, since even similar composites with higher fluorine content reacting with oxygen flow would show obvious signals from the remaining Al.[36] These unprecedented results indicate that FPUs can significantly enhance the combustion efficiency of AlNPs, encouraging us to examine the details of the combustion process.

Dynamic pressure characteristics of ETPUEs/AlNPs composites

A home-made test instrument including a closed steel bomb equipped with a piezoelectric pressure sensor, a quasi-static charge amplifiers and a mixed domain oscilloscopes was fabricated to research the combustion behavior of the ETPUEs/AlNPs composites. The instrument was set up according to literature method,[37] and a photograph of the instrument was

included in Fig. S9.† Dynamic pressure–time characteristics profiles were obtained by igniting the ETPUEs/AlNPs composites in air in a constant volume combustion bomb fitted with a pressure transducer. Representative pressure–time curves of the BDO-98-30/AlNPs and FPU-98-30/AlNPs composites are showed in Fig. 8a, and representative pressure–time curves of the FPUs/AlNPs composites in Fig. 8b. All the pressure-time curves progressed smoothly with time without obvious oscillations, indicating that the AlNPs were uniformly dispersed in the ETPUEs/AlNPs composites. Scanning electron microscopy (SEM) and energy dispersive X-ray spectroscopy (EDS) results confirmed the uniform dispersion of the AlNPs, as shown in Fig. S6 and S7.† A sharp increase in pressure appeared initially, which was followed by a gradual decay. As can be seen from Fig. 5a, the maximum pressure generated (P_{max}) from the combustion of the FPU-98-30/AlNPs composite was much higher than that from BDO-98-30/AlNPs composite, and the time to reach the maximum pressure (t_{mp}) was significantly shorter than that from BDO-98-30/AlNPs composite. This is because the fluorinated gas products produced by the decomposition of FPU-98-30 can react with AlNPs to further release energy. Interestingly, although the GAP content in FPUs decreased with an increasing hard segment content, their P_{max} from the combustion of FPUs/AlNPs composites only dropped slightly (Fig. 8b).

Besides P_{max} and t_{mp}, the maximum pressurization rate ($(dP dt^{-1})_{max}$) is also an important dynamic pressure characteristics, which can also be derived from the pressure-time curves. While P_{max} is a suggestive of the amount of energy released, and t_{mp} for the combustion rate, $(dP dt^{-1})_{max}$ is an indicator of the reactivity of the materials. The FPUs/AlNPs composites showed higher P_{max} and $(dP dt^{-1})_{max}$, and lower t_{mp} values than those from BDO-98-30/AlNPs composites. As shown by the comparison results in Fig. 8c, both FPU-98-35 and FPU-98-40 samples showed considerable $(dP dt^{-1})_{max}$, low t_{mp}, and high P_{max}, possibly due to the achievement of a delicate balance between
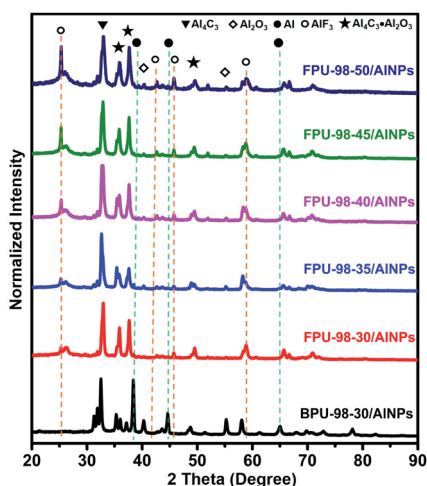

Fig. 7 Powder XRD patterns of the bomb calorimetry reaction products from the FPUs/AlNPs and BPU/AlNPs composites in argon.
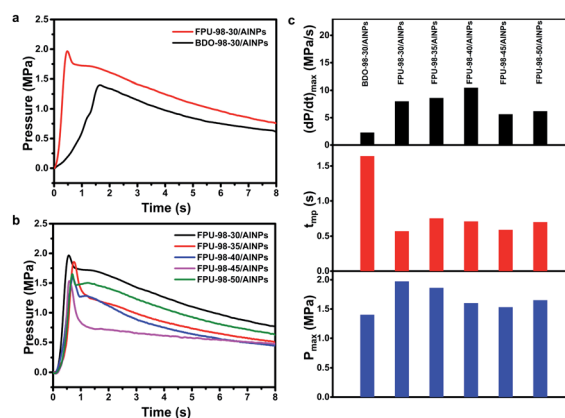

Fig. 8 Dynamic pressure characteristics of ETPUEs/AlNPs composites. (a) Pressure–time curves of BDO-98-30/AlNPs and FPU-98-30/AlNPs composites. (b) Pressure–time curves of FPUs/AlNPs composites. (c) Comparison of the performance derived from the dynamic pressure traces of the composites, $(dP dt^{-1})_{max}$ (up), t_{mp} (middle), P_{max} (bottom).

the content of energetic GAP soft segment and the fluorinated hard segment. From these results, it can be firmly concluded that FPUs can significantly improve the combustion efficiency of AlNPs and thus increase the amount of energy released from the energetic materials.

Kinetic simulations of FPUs/AlNPs composite from chemical reaction neural network

The combustion process of energetic nanocomposites is highly dynamic and complex, and a plausible reaction process is usually proposed based only on the analysis of starting materials and final products. In the current study, we used a recently-developed chemical reaction neural network (CRNN) approach to model the reaction kinetics.[38,39] The chemical reaction neural network model (CRNN) is a neural network modelling method to elucidate the reaction pathways and kinetic parameters by fitting the thermogravimetric experimental data.[39] In contrast to many other data-driven modelling approaches,[22,23] the CRNN model does not require the specific properties of experimental samples, and both reaction pathways (*e.g.* stoichiometric coefficients) and kinetic rate constants are considered as parameters in the optimization.

First, we incorporated the constraints from the thermal decomposition of FPUs/AlNPs into the framework of the CRNN model. The sample of FPU-98-40 is selected as the target in this work. Detailed modelling methods are included in the ESI.† By evaluating the prediction errors in the simulation results, the 5–5 model (involving 5 species and 5 reactions) was selected as the basis to reveal the possible reaction mechanism of FPUs/AlNPs composites. The comparisons between the prediction results of the 5–5 model and the TG experimental results with different heating rates are shown in Fig. 9. The predicted values are in excellent agreement with the experimental curves.

Fig. 10 shows the species evolution during the thermal decomposition of the FPUs/AlNPs composites, which was derived from the 5–5 model, and the corresponding reaction mechanism is included in Table 3. The 5 species and 5 reactions are termed "S_1, S_2, S_3, S_4, S_5" and "R_1, R_2, R_3, R_4, R_5", respectively. According to the reaction mechanism, S_3 and S_4 are intermediate substances in the overall reaction. The formation temperature of S_4 is approximately 200 °C, but it undergoes a quick decay in the conversion reaction. S_4 is all consumed at ~280 °C. The formation temperature of S_3 is also 200 °C, but it is sustained to a higher temperature. The mass fraction of S_3 diminishes to 0 at ~450 °C. S_2 and S_5 are the main products,
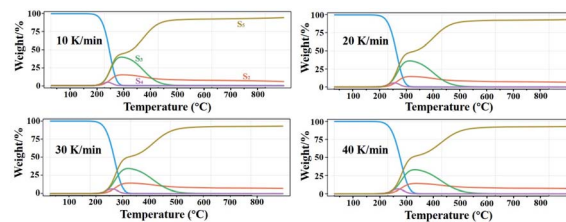
Fig. 10 Species evolution of FPUs/AlNPs composite during thermal decomposition predicted by the reaction mechanisms of the 5–5 model.

where S_2 and S_5 are the solid and gas products, respectively. S_5 shows two obvious growth steps within the temperature ranges of 200–280 and 280–450 °C before reaching a plateau. Its mass concentration is 85–90% in the final product for all four cases, and S_2 occupies ~10% in mass at ~500 °C and beyond.

Based on this 5–5 model, it can be deduced that the initial decomposition reaction R_1 of the FPUs/AlNPs system produces three substances, *e.g.* S_3, S_4 and S_5. Both R_2 and R_3 describe the decomposition of S_4, wherein the reaction rate of R_2 is approximately 1–2 orders of magnitude higher than that of R_3 (Fig. S4†). Therefore, R_3 is neglected in further analysis. R_2 yields three substances, S_2, S_3 and S_5. Both R_4 and R_5 produce S_2 and S_3. Because the reaction rate of R_5 is much higher than that of R_4, R_5 governs the reactions between S_2 and S_3, to form S_4. The stoichiometric coefficients of S_2 and S_3 are 1 and 4, respectively. This explains the fast decay of S_3 in Fig. 6b.

Combining the experimental observations (Fig. 3c and d) and the 5–5 model derived from the CRNN framework, the reaction mechanism of FPUs/AlNPs can subsequently be proposed in Fig. 11. R_1 is the main decomposition process of FPUs/AlNPs, producing relatively short (S_3) and long (S_4) fragments containing both fluorinated and polyether segments, and gas products (S_5). R_2 is the decomposition reaction of S_4, generating gas products (S_5) and solid substances (S_2 and S_3). R_4 and R_5 describe the decomposition reaction of the polyether segment (S_2) and short fragments containing both fluorinated and polyether segments (S_3). Both S_4 and S_3 are intermediate substances in the overall reaction. They are formed at a temperature of approximately 200 °C, which is consistent with previously reported experimental observations.[40] With a further increase in temperature, S_4 decomposes, mainly producing S_3 and partially producing S_5 with a small amount of solid carbon. S_3 decomposes to gas components (S_5) as the major product. In general, S_5 should represent a gaseous mixture including N_2, NH_3, C_xH_y, HCHO, HCN and C_xF_y. S_2 is the solid component, including polyether segments and solid carbon.

Since the CRNN model only considers the mass changes in the thermogravimetric data for learning, it is not capable of dealing with reactions without mass changes. As seen in the DSC results (Fig. 3c and d), a second peak appeared above 550–700 °C without mass loss. The possible reactions in this temperature range cannot be directly explained with CRNN models. Based on the above analysis, the reacting species below

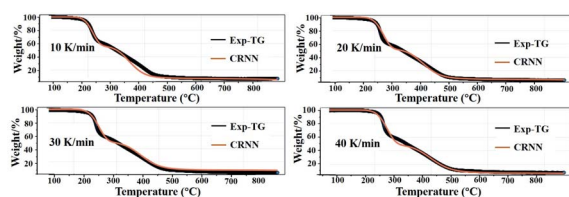**Fig. 9** The TG curves predicted by the CRNN models (red line) and experimental results (black line). The CRNN model here refers to the 5–5 model.

Paper

Table 3 Reaction mechanisms in the 5–5 model

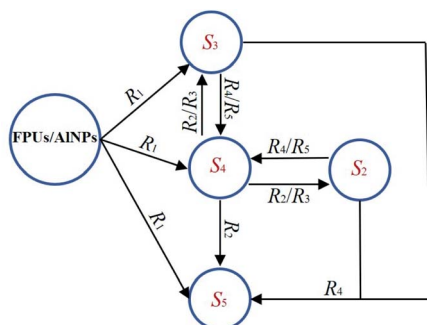| Reactions	Pathway	E_a (kJ mol^{-1})	n	ln A
R_1	$7 FPUs/AlNPs \rightarrow 1 S_3 + 4 S_4 + 2 S_5$	19.07	0.07	5.01
R_2	$8 S_4 \rightarrow 1 S_2 + 1.5 S_3 + 8 S_5$	20.27	0.36	4.99
R_3	$5 S_4 \rightarrow 1 S_2 + 4 S_3$	9.59	0.15	0
R_4	$7 S_2 + 5 S_3 \rightarrow 6 S_4 + 6 S_5$	34.39	0.02	0.76
R_5	$1 S_2 + 4 S_3 \rightarrow 5 S_4$	20.86	0.02	2.78

Fig. 11 Reaction network of the 5–5 model derived from CRNN framework.
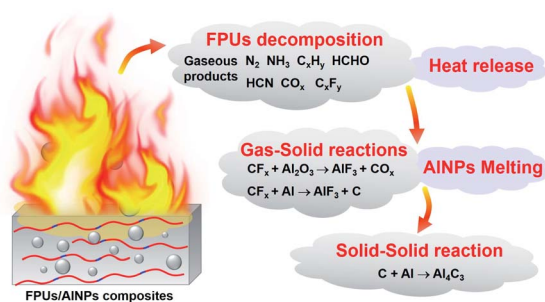

Fig. 12 A schematic illustration of the combustion reaction route of FPUs/AlNPs composites.

550 °C can be identified and thus the details of the combustion process can be proposed.

Discussion of the combustion process of the FPUs/Al composites

As we mentioned in the above section, the combustion of the FPUs/AlNPs composites is much more complicated than we initially expected. The amount of released energy is significantly larger than the additional enthalpy gain introduced by the exergonic reaction between the fluorinated component and AlNPs. Moreover, the combustion efficiency of AlNPs is also remarkably higher than those in other similar cases.[36] This may explain the extraordinary energy release from these composites.

Based on the above analysis and the information of the combustion products obtained from FPUs/AlNPs composites, a plausible reaction route can be proposed. During the initial stage in the range of 200–500 °C, FPU first decomposes to release gaseous products (e.g., N_2, NH_3, C_xH_y, HCHO, HCN,

C_xF_y) and solid products (polyether segments and carbon).[41–44] The excessive heat released from the decomposition of azide groups in GAP units greatly facilitated the melting of AlNPs, and thus enhanced the energy propagation in the composites via the so-called "melt dispersion mechanism (MDM)" in the next stage (500–660 °C).[33,45,46] During the second stage, the gaseous products reacted with AlNPs. Especially, the fluorinated gaseous products reacted with alumina to expose reactive aluminum surface. Owing to the uniform dispersion of fluorinated components inside the composites, this phenomenon occurred homogeneously and consequently improved the combustion of AlNPs significantly. In the final stage (above 660 °C), the melted nano-aluminum started to react with solid products decomposed from FPUs to finally release a tremendous amount of heat, which in return assisted the melting of AlNPs to reach nearly full consumption.

A schematic illustration of this reaction mechanism is included in Fig. 12. Our results suggest that the energetic component and fluorinated component decompose independently at different stages during the combustion of FPUs/AlNPs composites. However, when these two are combined in one FPU, the heat released from the decomposition energetic component facilitated the melting of AlNPs, and the reactive species from the decomposition of the fluorinated component reacted with the retardant alumina layer, exposing more aluminum surface for further reaction. These two effects work synergistically to facilitate the energy propagation in composites, resulting in significantly improved combustion efficiency of AlNPs and tremendously enhanced energy release from the composites.

Conclusions

In the current study, a series of aluminum nanoparticle-based energetic composites with fluorinated energetic polyurethanes as binder were prepared, and their properties and performance were carefully evaluated. These polyurethanes could endow the composites with decent and tunable mechanical properties. More importantly, the application of these fluorinated and energetic polyurethanes as binders for energetic composites with aluminum nanoparticles could significantly improve the combustion efficiency of the metallic fuels, and enhance the energy release from the energetic composite materials at the same time, revealing great potential in the application of energetic materials. A detailed combustion mechanism was identified based on the analysis of combustion products and chemical reaction neural network model. It was found that the

energetic and fluorinated components work synergistically during the decomposition process to facilitate energy propagation in aluminum nanoparticles, which is the key for such high-performance energetic composites. It can be envisioned that these fluorinated energetic polyurethanes will surely be very useful in the field of energetic composite materials such as thermite, solid propellants, explosives, pyrotechnics, and so on.[47,48]

Author contributions

G. T. carried out all the synthesis, preparation and most of characterization experiments. H. W., Y. B. X., and D. P. C. helped with kinetic simulations. C. Y. C and D. L. W. helped with some characterization experiments. X. Y. L. designed and supervised the project. The manuscript was written by X. Y. L. and G. T.

Conflicts of interest

The authors declare that they have no known competing financial interests or personal relationships that could have appeared to influence the work reported in this paper.

Acknowledgements

Notes and references

1 A. Davenas, *J. Propul. Power*, 2003, **19**, 1108–1128.
2 H. Nie, L. P. Tan, S. Pisharath and H. H. Hng, *Chem. Eng. J.*, 2021, **414**, 128786.
3 S. Wang, Q. Wang, X. Feng, B. Wang and L. Yang, *Adv. Mater.*, 2017, **29**, 1701898.
4 Q. Zhang and J. n. M. Shreeve, *Angew. Chem., Int. Ed.*, 2014, **53**, 2540–2542.
5 J. Yang, G. Zhang, J. Wang, Y. Hao, G. Hao, L. Xiao, J. Chen, B. Zhou, J. Fu and W. Jiang, *J. Mater. Chem. A*, 2021, **9**, 16076–16085.
6 J. Li, K. Liu, Y. Gao, S. Liu, W. Wang and Y. Liu, *J. Propul. Power*, 2018, **34**, 1198–1205.
7 K. B. Plantier, M. L. Pantoya and A. E. Gash, *Combust. Flame*, 2005, **140**, 299–309.
8 R. A. Yetter, G. A. Risha and S. F. Son, *Proc. Combust. Inst.*, 2009, **32**, 1819–1838.
9 N. H. Yen and L. Y. Wang, *Propellants, Explos., Pyrotech.*, 2012, **37**, 143–155.
10 E. Tang, S. Li, C. Chen and Y. Han, *J. Mater. Res. Technol.*, 2020, **9**, 8391–8400.
11 E. A. Cadwallader, *US Pat.*, US56631756A, 1964.
12 K. B. Rider, B. K. Little, S. B. Emery and C. M. Lindsay, *Propellants, Explos., Pyrotech.*, 2013, **38**, 433–440.
13 L. Wang, J. Liu, S. Li and X. Zhang, *AIP Adv.*, 2015, **5**, 117142.
14 M. Losada and S. Chaudhuri, *J. Phys. Chem. A*, 2009, **113**, 5933–5941.
15 Z. Liu, Y. Zhang, Q. Zhou, R. Chen and S. Guo, *J. Appl. Polym. Sci.*, 2022, 52153.
16 H. E. Kissinger, *J. Res. Natl. Bur. Stand.*, 1956, **4**, 217–221.
17 H. L. Friedman, *J. Polym. Sci., Part C: Polym. Symp.*, 1964, **6**, 183–195.
18 T. Ozawa, *Bull. Chem. Soc. Jpn.*, 1965, **38**, 1881–1886.
19 M. J. Starink, *Thermochim. Acta*, 2003, **404**, 163–176.
20 J. A. Blasco, N. Fueyo, C. Dopazo and J. Ballester, *Combust. Flame*, 1998, **113**, 38–52.
21 K. Luo, J. Xing, Y. Bai and J. Fan, *Combust. Flame*, 2018, **193**, 283–294.
22 C. Chi, G. Janiga and D. Thévenin, *Combust. Flame*, 2021, **226**, 467–477.
23 L. L. C. Franke, A. K. Chatzopoulos and S. Rigopoulos, *Combust. Flame*, 2017, **185**, 245–260.
24 Z. Zhang, G. Wang, Z. Wang, Y. Zhang, Z. Ge and Y. Luo, *Polym. Bull.*, 2015, **72**, 1835–1847.
25 Y. Hu, G. Tang, Y. Luo, S. Chi and X. Li, *Polym. Chem.*, 2021, **12**, 4072–4082.
26 G. Tang, D. Wang, Y. Luo and X. Li, *Eur. Polym. J.*, 2022, **177**, 111428.
27 K. W. Watson, M. L. Pantoya and V. I. Levitas, *Combust. Flame*, 2008, **155**, 619–634.
28 J. McCollum, M. L. Pantoya and S. T. Iacono, *J. Fluorine Chem.*, 2015, **180**, 265–271.
29 Y. Hu, D. Hao, B. Tao, F. Wang, D. Wang, R. Fan, D. Xia, P. Wang, Y. Yang, A. Pang and K. Lin, *Chem. Eng. J.*, 2020, **394**, 124884.
30 Z. Li, X. Zhao, G. Li, F. Gong, Y. Liu, Q. Yan, Z. Yang and F. Nie, *Chem. Eng. J.*, 2021, **425**, 131619.
31 Y. Ou, Q. Jiao, N. Li, S. Yan and R. Yang, *Chem. Eng. J.*, 2021, **403**, 126367.
32 E. M. Hunt, S. Malcolm, M. L. Pantoya and F. Davis, *Int. J. Impact Eng.*, 2009, **36**, 842–846.
33 O. Mulamba and M. L. Pantoya, *Appl. Surf. Sci.*, 2014, **315**, 90–94.
34 M. Jin, G. Wang, J. Deng, G. Li, M. Huang and Y. Luo, *J. Sol-Gel Sci. Technol.*, 2015, **76**, 58–65.
35 S. K. Valluri, M. Schoenitz and E. L. Dreizin, *J. Mater. Sci.*, 2017, **52**, 7452–7465.
36 H. A. Miller, B. S. Kusel, S. T. Danielson, J. W. Neat, E. K. Avjian, S. N. Pierson, S. M. Budy, D. W. Ball, S. T. Iacono and S. C. Kettwich, *J. Mater. Chem. A*, 2013, **1**, 7050–7058.
37 C. Sang, K. Chen, G. Li, S. Jin and Y. Luo, *RSC Adv.*, 2021, **11**, 7633–7643.
38 W. Ji, F. Richter, M. J. Gollner and S. Deng, *Combust. Flame*, 2022, **240**, 111992.
39 W. Ji and S. Deng, *J. Phys. Chem. A*, 2021, **125**, 1082–1092.
40 H. Arisawa and T. B. Brill, *Combust. Flame*, 1998, **112**, 533–544.
41 Y. Oyumi and T. B. Brill, *Combust. Flame*, 1986, **65**, 127–135.
42 H. Fazlıoğlu and J. Hacaloğlu, *J. Anal. Appl. Pyrolysis*, 2002, **63**, 327–338.

43 T. Wang, S. Li, B. Yang, C. Huang and Y. Li, *J. Phys. Chem. B*, 2007, **111**, 2449–2455.

44 J. Zhang, J. Huang, X. Fang, Y. Li, Z. Yu, Z. Gao, S. Wu, L. Yang, J. Wu and J. Kui, *Materials*, 2018, **11**, 2451.

45 V. I. Levitas, B. W. Asay, S. F. Son and M. Pantoya, *Appl. Phys. Lett.*, 2006, **89**, 071909.

46 R. K. Walzel, V. I. Levitas and M. L. Pantoya, *Powder Technol.*, 2020, **374**, 33–39.

47 T. Jarosz, A. Stolarczyk, A. Wawrzkiewicz-Jalowiecka, K. Pawlus and K. Miszczyszyn, *Molecules*, 2019, **24**, 4475.

48 A. Kanti Sikder and S. Reddy, *Propellants, Explos., Pyrotech.*, 2013, **38**, 14–28.